

Diurnal Variability of the Radiative Impact of Atmospheric Aerosols in Ouagadougou, Burkina Faso: A Seasonal Approach

Bruno Korgo^{1*}, Bernard Zouma¹, Pétronille Kafando², Nebon Bado¹, Martial Zoungrana¹, Issa Zerbo¹, Jean-Claude Roger³, Joseph D. Bathiebo¹

¹Laboratory of Thermal and Renewable Energy, Department of Physics, University Joseph KI-ZERBO, Ouagadougou, Burkina Faso

²Laboratory of Environmental Physics and Chemistry, Department of Physics, University Joseph KI-ZERBO, Ouagadougou, Burkina Faso

³University of Maryland, Department of Geographical Sciences, College Park, USA

Email: *brunokor@yahoo.fr

How to cite this paper: Korgo, B., Zouma, B., Kafando, P., Bado, N., Zoungrana, M., Zerbo, I., Roger, J.-C. and Bathiebo, J.D. (2020) Diurnal Variability of the Radiative Impact of Atmospheric Aerosols in Ouagadougou, Burkina Faso: A Seasonal Approach. *Journal of Environmental Protection*, 11, 1089-1102.

<https://doi.org/10.4236/jep.2020.1112069>

Received: November 24, 2020

Accepted: December 28, 2020

Published: December 31, 2020

Copyright © 2020 by author(s) and

Scientific Research Publishing Inc.

This work is licensed under the Creative

Commons Attribution International

License (CC BY 4.0).

<http://creativecommons.org/licenses/by/4.0/>



Open Access

Abstract

The objective of this work is to study the diurnal evolution of the radiative impact of atmospheric aerosols in an urban city located in the West African Sahel and the correlations with the main influencing factors of local climate dynamics. The simulation was performed using a treatment chain including the GAME code. In the methodology, the atmosphere is modeled by 33 plane parallel layers and the effects of absorption, multiple scattering by particles and gas are taken account. An hour-by-hour calculation of radiative forcing at the top of the atmosphere, in the atmospheric layer and at the earth's surface was performed. The data used as input are the monthly averages of optical properties, radiosonde measurements, daily synoptic measurements and surface albedo. The results show a parabolic diurnal course of a negative radiative impact at the top of the atmosphere with an extremum at 12 o'clock. Maximum cooling is observed shortly after sunrise and shortly after sunset. The largest annual deviations are noted between the months of March and December with respective maximum cooling values of -34 W/m^2 and -15.60 W/m^2 . On the earth's surface, a cooling impact is observed with two diurnal peaks at sunrise and sunset, the greatest difference between the diurnal maximums is noted between March (-104.45 W/m^2) and August (-54 W/m^2). In the atmospheric layer, there is almost constant diurnal warming between 9 a.m. and 4 p.m. The maximum difference between the diurnal extremes is also noted between March (about 85 W/m^2) and August (35 W/m^2). Likewise, the study of the diurnal warming of the first atmospheric layer showed the extreme values in March (5.6°C) and August (2.4°C), these maximum values

being always observed at around 12 o'clock. An analysis of similar works carried out in urban cities in various locations of the world has shown a relatively good accordance with the values obtained. This study highlights the radiative impact of Saharan desert dust, the effect of the local climate and the succession between dry season (November to May) and the rainy one (July to October), as well as the zenith solar angle and human activity.

Keywords

AERONET, Optical Properties, Radiative Forcing, Harmattan, Monsoon, Sahara Desert

1. Introduction

Ouagadougou is the capital of Burkina Faso, a landlocked country in West Africa bordering in its northern part with the Sahara Desert. With approximately 8.5 million km² [1] the Sahara is recognized as the largest desert of the earth and the world's leading source of desert aerosols. Several studies estimate 400 and 700 Mt [2] [3] [4] [5], the contribution of emissions from the Sahara. Ouagadougou, like the entire Sahelian zone, is strongly impacted by these important emissions which significantly affect the optical and microphysical properties of aerosols [6]. This situation directly affects the radiative properties of atmospheric aerosols in the city of Ouagadougou, which is also subject to the effect of emissions linked to human activity. Numerous studies have highlighted the combined effects of the climatic season and human activity on the composition and properties of aerosols in large urban cities [7] [8]. The objective of this work is to study, the monthly evolution of the diurnal radiative forcing in Ouagadougou as well as the influence of the seasonal variability of the West African climate.

2. Methodology

The calculation methodology is a simulation realized by a treatment chain which includes the GAME code, "Global Atmospheric Model" [9]. The simulation of the aerosol radiative forcing is carried out according to a model of atmosphere divided into 33 plane and parallel layers. The calculation is performed with the line by line method [10], takes into account the effect of shortwave absorbers in the electromagnetic spectrum [11], and deals with multiple scattering problems by the discrete ordinate method [12] as well as interactions between multiple scattering and gas absorption [13]. Specifically, the methodology integrates the effects of all particle-radiation interactions in the atmosphere, namely:

- Absorption by gases, H₂O, O₂, CO₂, O₃.
- The Rayleigh scattering by molecules.
- Absorption by aerosols through the single scattering albedo.
- Diffusion due to aerosols by the asymmetry factor.
- The surface albedo.

The treatment chain gives the following output:

- Direct radiative forcing at the top of the atmosphere F_{TOA} :

$$\Delta F_{TOA} = F_{TOA}^a - F_{TOA}^0 \quad (1)$$

- Direct radiative forcing at the surface ΔF_{BOA} :

$$\Delta F_{BOA} = F_{BOA}^a - F_{BOA}^0 \quad (2)$$

- Radiative forcing in the atmospheric layer ΔF_{ATM} which is a simple difference between radiative forcing at the top of the atmosphere and at the earth's surface

$$\Delta F_{ATM} = \Delta F_{TOA} - \Delta F_{BOA} \quad (3)$$

In the above expressions, F_{TOA}^a and F_{BOA}^a are the net fluxes calculated at the top of the atmosphere and at the surface, respectively, taking into account the impact of aerosol; F_{TOA}^0 and F_{BOA}^0 are respectively the net fluxes at the top of atmosphere and at the surface calculated without the effect of aerosols.

- The vertical profile of the determined heating rate is calculated from the following thermodynamic relationship [11]:

$$\frac{\partial T}{\partial t} = -\frac{1}{\rho C_p} \frac{\partial F(z)}{\partial z} \quad (4)$$

where T denotes the air temperature, and t the time.

ρ is the density of the atmosphere.

C_p is the specific heat of the air.

$F(z)$ is the net flux at altitude z .

3. Data

The methodology uses several data sets as input. These include the optical properties of aerosols, vertical temperature and humidity profiles, ambient temperatures, surface albedo and solar angle.

3.1. Optical Properties

The optical data used in this work are optical thicknesses, Angstrom's exponent, and Single Scattering Albedo (SSA). These data are extracted from the database of photometric measurements and inversion products of "Aerosol RObotic NETwork" (AERONET) [14]. In Ouagadougou, the measurements were carried out from 1999 to 2007. All the data were the subject of a qualitative analysis and monthly averages were calculated using the sorted data to better perceive the impact of the climate seasonal dynamics in West Africa.

The optical thicknesses are measured on 4 channels (440 nm, 675 nm, 870 nm and 1020 nm). The Angström exponent is calculated over the wavelength range of 440 nm to 870 nm, covering almost the entire band of atmospheric radiation (Table 1). This coefficient makes it possible to deduce, over all wavelengths of the interval, the optical thickness of the aerosols.

The single scattering albedo is a key parameter in assessing the radiative impact of an aerosol population as it perfectly describes the scattering character relatively to the aerosol absorbency. The monthly averages used in this study are presented in **Table 2**.

Table 1. Monthly averages of optical thicknesses and Angstrom's exponent.

| | AOT ₁₀₂₀ | AOT ₈₇₀ | AOT ₆₇₅ | AOT ₄₄₀ | 440 - 870 Angstr |
|-----|---------------------|--------------------|--------------------|--------------------|------------------|
| JAN | 0.37 | 0.40 | 0.45 | 0.52 | 0.41 |
| FEB | 0.51 | 0.55 | 0.59 | 0.66 | 0.37 |
| MAR | 0.73 | 0.77 | 0.81 | 0.85 | 0.20 |
| APR | 0.52 | 0.55 | 0.58 | 0.64 | 0.25 |
| MAY | 0.50 | 0.53 | 0.55 | 0.58 | 0.20 |
| JUN | 0.49 | 0.52 | 0.55 | 0.59 | 0.26 |
| JUL | 0.31 | 0.35 | 0.37 | 0.44 | 0.47 |
| AUG | 0.35 | 0.38 | 0.40 | 0.46 | 0.39 |
| SEP | 0.28 | 0.30 | 0.33 | 0.39 | 0.48 |
| OCT | 0.38 | 0.41 | 0.45 | 0.52 | 0.40 |
| NOV | 0.27 | 0.29 | 0.33 | 0.39 | 0.49 |
| DEC | 0.22 | 0.25 | 0.28 | 0.35 | 0.59 |

Table 2. Monthly averages of the single scattering albedo.

| | SSA _{441-T} | SSA _{673-T} | SSA _{873-T} | SSA _{1022-T} |
|-----|----------------------|----------------------|----------------------|-----------------------|
| JAN | 0.86 | 0.91 | 0.92 | 0.92 |
| FEB | 0.89 | 0.94 | 0.95 | 0.95 |
| MAR | 0.90 | 0.96 | 0.96 | 0.97 |
| APR | 0.90 | 0.95 | 0.95 | 0.95 |
| MAY | 0.91 | 0.95 | 0.95 | 0.95 |
| JUN | 0.90 | 0.96 | 0.96 | 0.96 |
| JUL | 0.89 | 0.92 | 0.92 | 0.92 |
| AUG | 0.93 | 0.95 | 0.96 | 0.96 |
| SEP | 0.90 | 0.93 | 0.94 | 0.94 |
| OCT | 0.91 | 0.95 | 0.95 | 0.95 |
| NOV | 0.89 | 0.93 | 0.94 | 0.94 |
| DEC | 0.86 | 0.90 | 0.90 | 0.91 |

3.2. Vertical Temperature and Humidity Profiles in Ouagadougou

Vertical temperature and humidity profiles were obtained from radiosonde data measured daily. We used the averages of the 2006 measurements because this year corresponds to the period where the photometric data were the most abundant and regular in Ouagadougou.

The vertical temperature profile shows an almost linear tropospheric layer extending from the surface to about 17,000 meters. A climatology of the data has shown that the average gradient of $6^{\circ}\text{C}/\text{km}$ in the case of a standard atmosphere seems to adequately describe the vertical temperature profile in Ouagadougou although it is necessary to note some slight differences according to the seasons due to the presence of varying degrees of water vapor, clouds, etc. (Figure 1).

The first layer is the most interesting for us because it is at this level that almost all atmospheric aerosols, subject of our study, are concentrated. The upper layers present very little interest in our work.

While the vertical temperature profile is stable over most of the year, the humidity profile fluctuates widely (Figure 2). For our study, approximations were performed by analyzing the general trend of month-to-month measurements. Average values were therefore set for each specific altitude band.

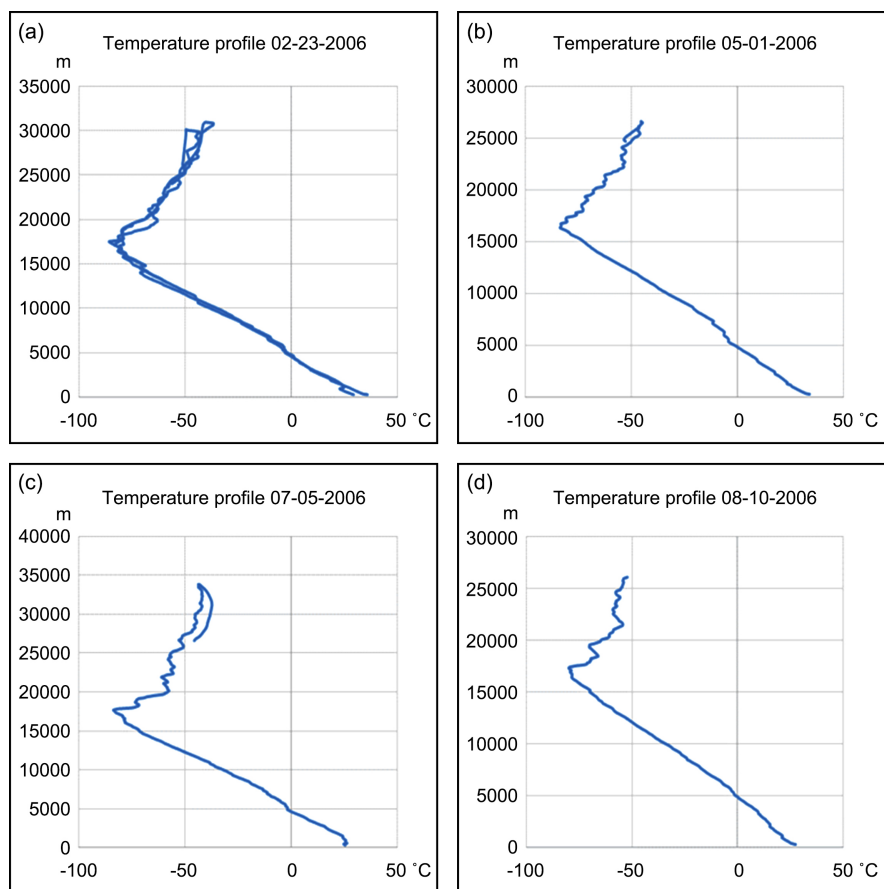


Figure 1. Illustration of vertical temperature profiles in dry (a), (b) and humid season (c), (d) in Ouagadougou.

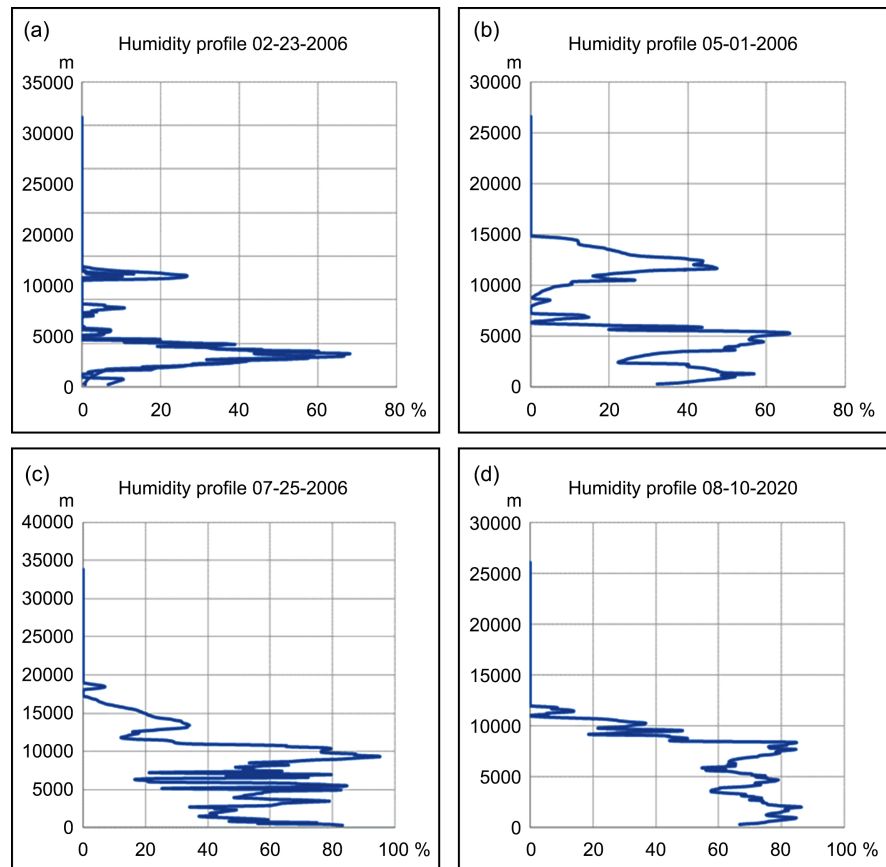


Figure 2. Illustration of vertical humidity profiles in dry season (a), (b) and humid season (c), (d) in Ouagadougou.

Figure 2 shows a totally dry atmosphere in the upper part (beyond 15 km). In the lower part, there are several successive series of increasing and decreasing variations of relative humidity. Average surface values of around 30% to 40% in the dry period and 70% to 80% in the rainy season are noted.

3.3. Daytime Ambient Temperature and Surface Albedo

The daily variation of ambient temperature is key in evaluating the hourly radiative forcing in the period between sunrise and sunset. In Ouagadougou as in the entire Sahelian zone, in general the ambient temperature during the day has a parabolic form, with a minimum depending on the season between 20°C and 25°C at 5 a.m. to 6 a.m. in the morning and the maximum at 12 p.m. to 1 p.m. with mean values of 30°C and 35°C (sometimes higher in the hot period of March-April-May). We used in this work, the synoptic data averaged hour by hour.

As for the surface albedo, also called the reflection factor, which expresses the fraction of the radiation reflected by the earth's surface, we estimated it from the MODIS (Moderate Resolution Imaging Spectroradiometer) sensor products which gives the spectral dependence of the albedo surface at seven wavelength bands [15].

4. Results

4.1. Diurnal Evolution of the Radiative Impact

In this paragraph, we make an hour-by-hour estimate of the radiative impact at the top of the atmosphere (TOA), on the earth's surface (BOA) as well as in the atmospheric layer (ATM) for each month of the year. This helps to understand the evolution of the impact of aerosols between sunrise and sunset. The results of the calculations are presented by the curves in **Figure 3** below.

4.1.1. At the Top of the Atmosphere

At the top of the atmosphere, the diurnal trend of the radiative impact of aerosols is negative, which generally reflects cooling. The analysis of the diurnal variability of this impact shows a parabolic evolution with maximum daily cooling values in the first hours after sunrise and in the last hours before sunset. These values are recorded in the morning around 7 a.m. and at the end of the afternoon, around 5 p.m. Note that the sun rises on average at 6 a.m. and sets around 6 p.m. Depending on the season, a shift of a few minutes around these times can be observed. The cooling gradually decreases during the day and reaches its minimum value around 12 o'clock. Low positive forcing values are observed over several months between 11 a.m. and 1 p.m. This time slot coincides with the maximum solar radiation.

The annual analysis shows a maximum cooling in March of -34 W/m^2 , the trend continues in April-May and June before decreasing. The lowest values of cooling were noted in December (-15.60 W/m^2) and January (-18.15 W/m^2).

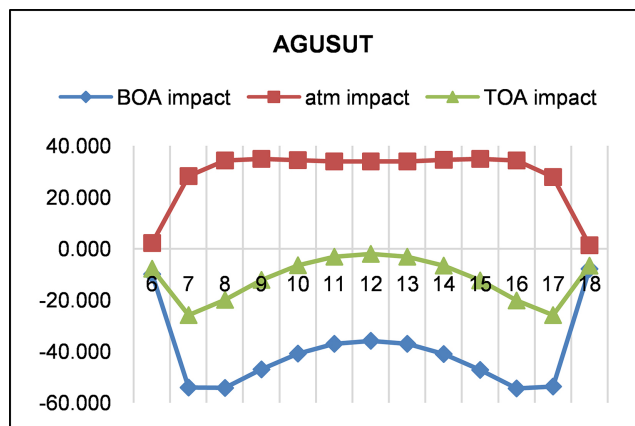
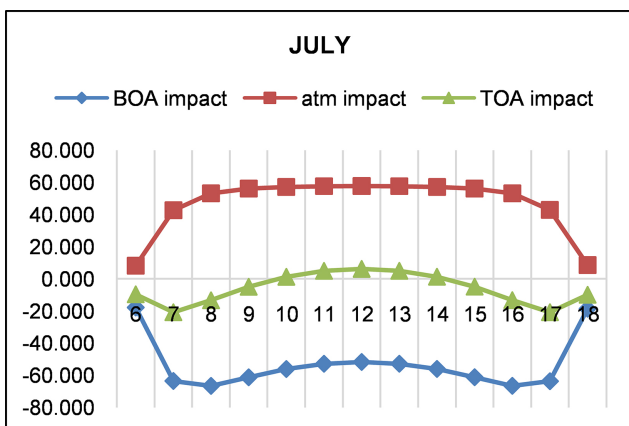
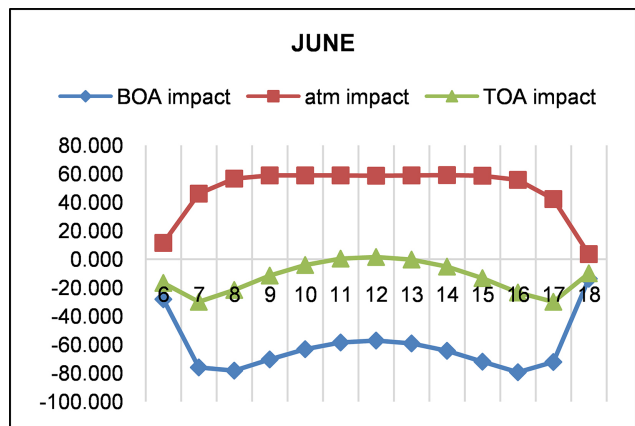
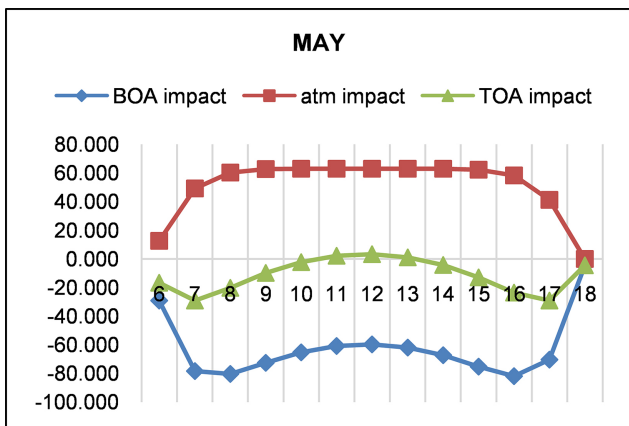
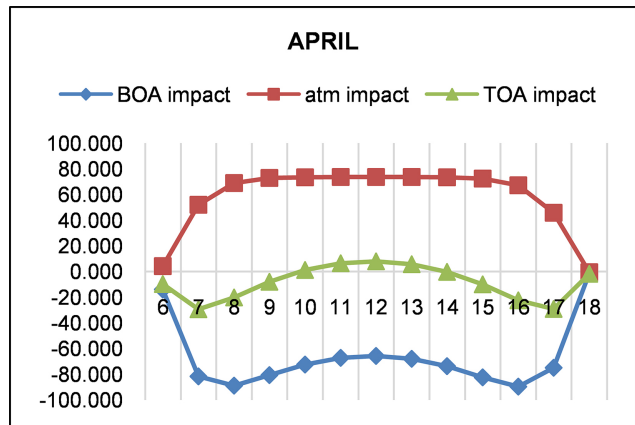
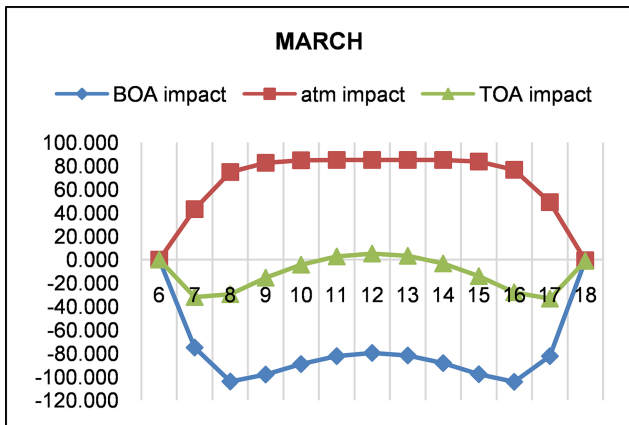
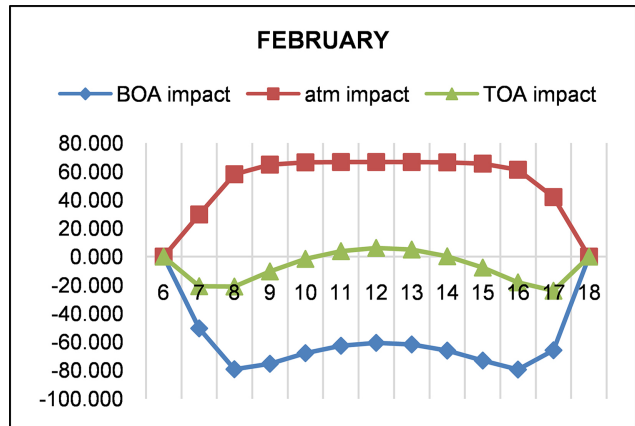
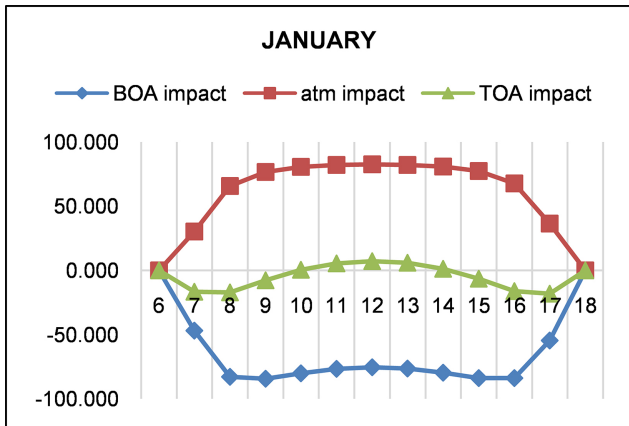
4.1.2. At the Surface

The radiative forcing at surface is negative throughout the year. The diurnal evolution of this forcing has the same look throughout the year. The curves show two neighboring peaks shortly after sunrise (between 7 a.m. and 8 a.m.) and shortly before sunset (between 4 p.m. and 5 p.m.). We can logically think of the effect of human activity and the emission peaks it causes in the morning and late afternoon, but also of the effect of the dynamics of air masses and turbulence created by the warming of the surface at sunrise and onset of cooling in the evening. The minimum cooling is observed around 12 o'clock, when the sun is at the zenith and the solar flux is greater.

The results also show that the maximum daily values of cooling range from -104.45 W/m^2 in March to -54.60 W/m^2 calculated in August.

4.1.3. In the Atmospheric Layer

The cooling of the surface is the logical consequence of a warming in the atmospheric layer. In the atmosphere, the calculated positive forcing is the effect of a significant absorption of radiation by aerosols strongly impacted by human activity during the day. On a daily scale, this warming varies increasingly from sunrise until around 9 a.m. From that moment the forcing remains almost constant until the afternoon between 3 p.m. and 4 p.m. before experiencing a decrease until sunset.



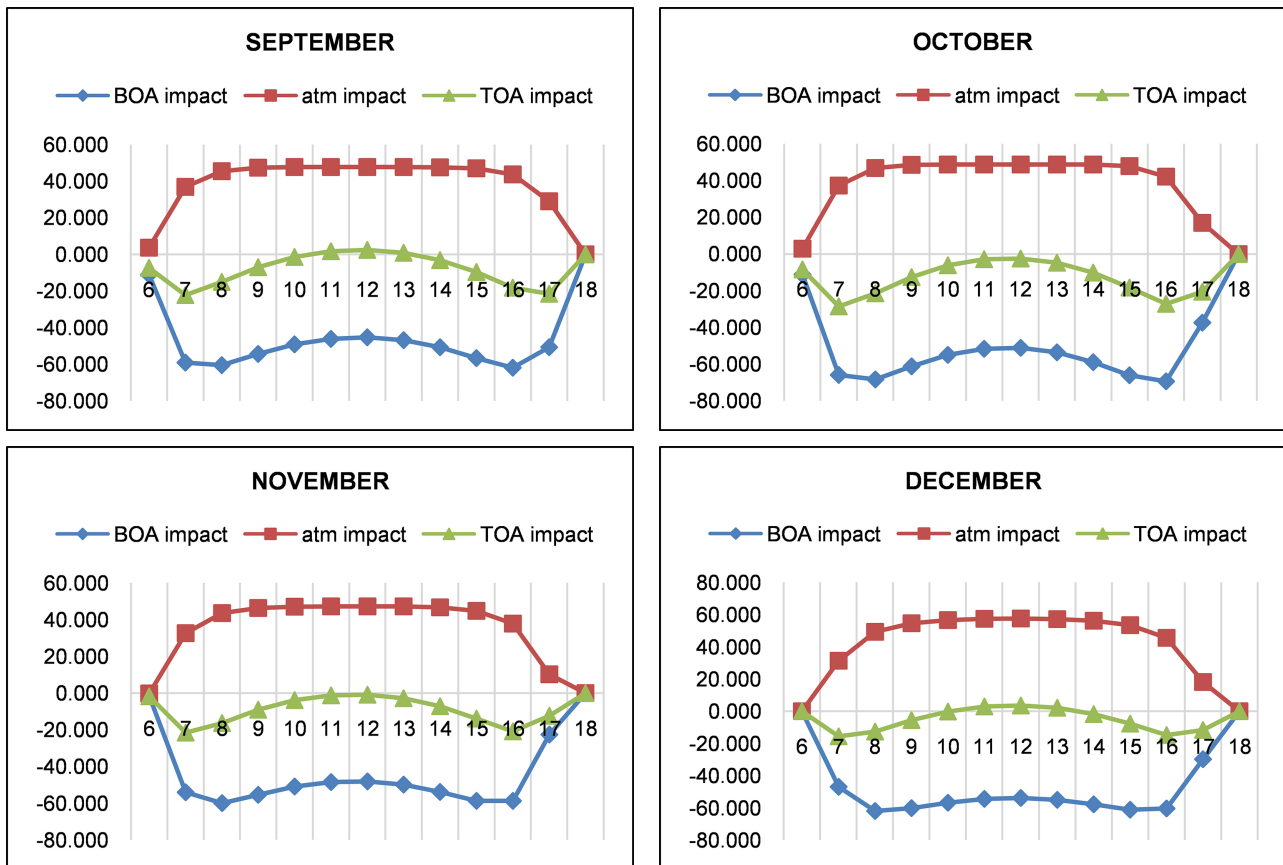


Figure 3. Monthly averages of diurnal evolution of the radiative impact at the top of the atmosphere (TOA), in the atmosphere (ATM) and at the surface (BOA).

The annual variability is marked by extreme values calculated in March where the warming is maximum (around $85 W/m^2$ calculated) and in August where it is minimal with a value found around $35 W/m^2$.

4.2. Seasonal Analysis of the Diurnal Radiative Impact

The variability of the diurnal radiative impact at the top of the atmosphere, in the atmospheric layer and on the Earth's surface shows a strong correlation with West African climate dynamics. In fact, the climate in West Africa south of the Sahara is punctuated by the succession of monsoon and harmattan flows separated by a front line, the intertropical front whose latitudinal rise and fall brings the rainy season in its North and South part. In the Sahelian zone, the dry season sets in from October to May and gives way to the rainy season which follows it from June to September. August is recognized as the month with the highest rainfall in the year in the Sahel. The optical and microphysical properties of aerosols in Ouagadougou and in the Sahel are strongly impacted by this seasonal succession. The Northeast Harmattan flow from the dust-laden Sahara Desert significantly marks the aerosol population in the lower atmospheric layers in Ouagadougou during the dry season. Conversely, the monsoon flow from the humid South brings rains which have a leaching effect on the suspension of

desert dust which is reduced [6]. Thus, the extreme values of diurnal radiative forcings observed within the atmospheric layer and on the surface in March and August are logically the effect of West African climate dynamics. The month of March is optically characterized by the effect of strong dust suspensions and high values of optical thicknesses and the month of August by the lowest values. At the top of the atmosphere, the annual variability suggests the combined effect of the local climate and also of the large-scale dynamics between North and South. This explains the extreme values seen in March and then in December and not in August. **Figure 4**, **Figure 5** and **Figure 6** illustrate the differences between diurnal forcings in March and August, highlighting the effect of local dynamics.

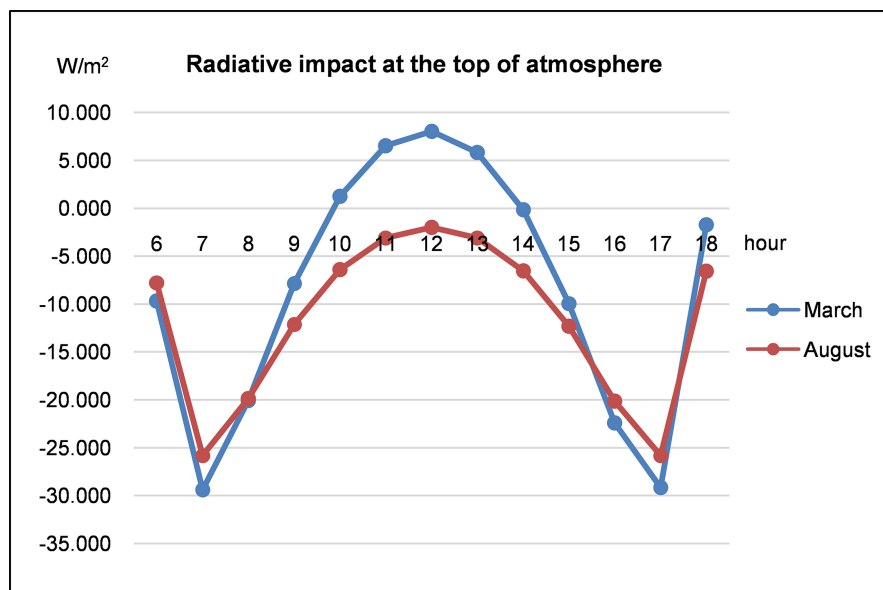


Figure 4. The hourly radiative impact at the top of the atmosphere in March and August.

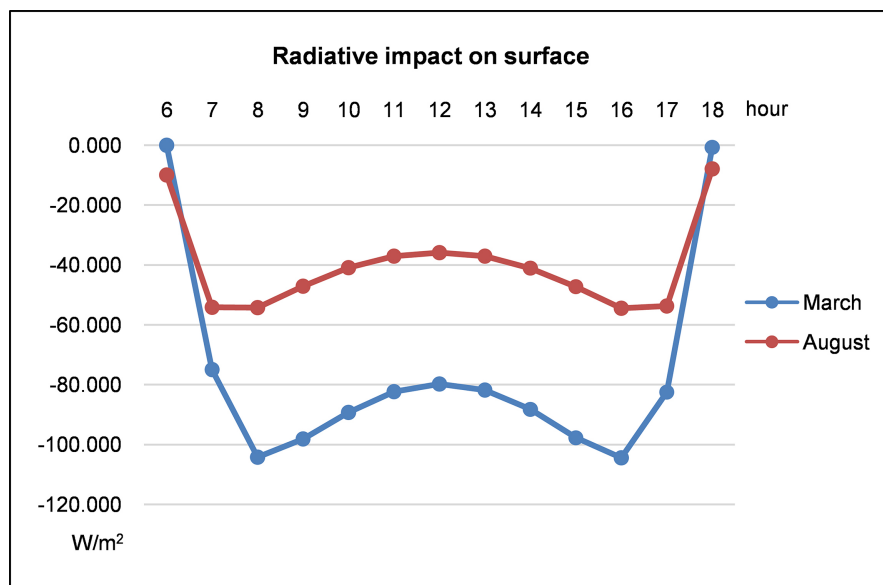


Figure 5. The hourly radiative impact at the surface in March and August.

The diurnal evolution of warming at the first atmospheric layer (in contact with the surface) was calculated and analyzed in this study. The diurnal variability shows a parabolic pattern from sunrise to sunset. The maximum daytime values are observed around 12 noon. The annual analysis showed, like the radiative forcings, the very marked influence of the local West African climate as shown in **Figure 7**. The highest diurnal maximum values were recorded in the dry season, particularly in March (5.60°C) and the lowest value in August during the rainy season (2.4°C).

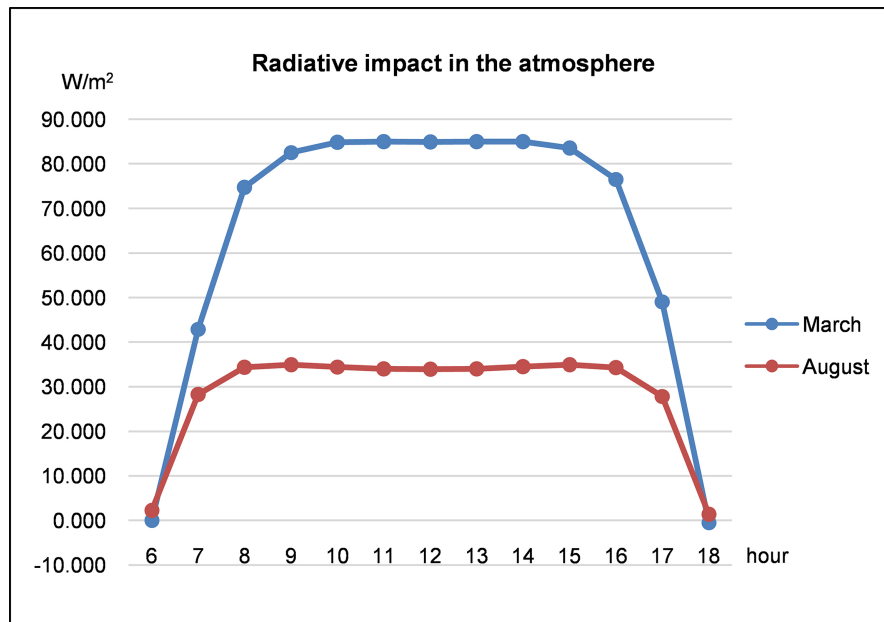


Figure 6. The hourly radiative impact within the atmospheric layer in March and August.

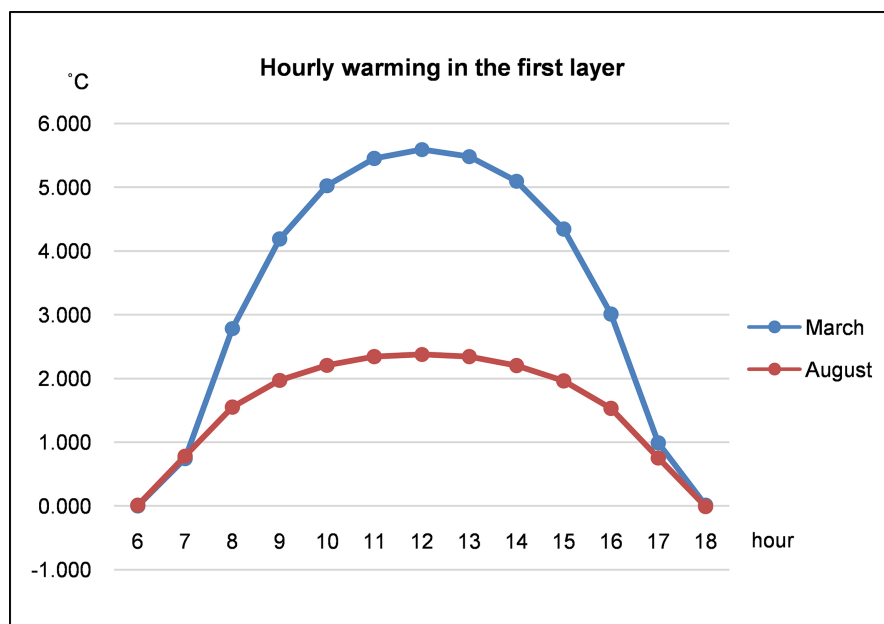


Figure 7. Hourly warming in the first layer in March and August.

5. Discussion

By various methods, and at different space and time scales, radiative forcing calculations have been reported in the literature. All studies show a negative radiative impact at the top of the atmosphere and at the surface, then a positive impact in the atmospheric layer.

Specifically, in the West African region, similar work has been carried out [16] [17] [18]. The results show average values of cooling at the top of the atmosphere which can range from -3 W/m^2 to -17.5 W/m^2 , values of heating in the atmospheric layer which can reach more than 30 W/m^2 and values of cooling in surface ranging from -10 W/m^2 to more than -57 W/m^2 .

At the scale of an urban city, studies have been conducted in regions with different climatic situations and whose aerosol optical properties have different influences and characteristics from the West African context. Recent studies conducted in Beijing [19], estimate a radiative forcing varying between -6.69 and -235 W/m^2 (with an average of $-54.93 \pm 39.92 \text{ W/m}^2$) at the surface and an average of $35.56 \pm 22.88 \text{ W/m}^2$ in the atmosphere. In the same way, [20] found a monthly average radiative forcing at the earth's surface and at the top of the atmosphere which varies from -40 ± 7 to $-105 \pm 25 \text{ W/m}^2$ and from -18 ± 4 at $-49 \pm 17 \text{ W/m}^2$ respectively. The maximum atmospheric warming was found to be $66 \pm 12 \text{ W/m}^2$. In the Karashi mega-city, [21] estimated the radiative forcing of aerosols at the top of the atmosphere of around -7 to -35 W/m^2 (average $-22 \pm 6 \text{ W/m}^2$), at the surface of -56 to -96 W/m^2 (average $-73 \pm 12 \text{ W/m}^2$) and a positive forcing in the atmosphere of $+38$ to $+61 \text{ W/m}^2$ (average $+51 \pm 13 \text{ W/m}^2$).

The analysis of these results shows overall consistency with our study even if some observed differences can be justified in the geographical location, climatic influences, socio-economic activity and methodological approach. In fact, our assessment of the diurnal variation is based on the monthly averages of the input data (optical properties, atmospheric thermodynamic measurements, ambient temperatures, etc.) to better understand the impact of the local climate. An assessment with real-time data would certainly have presented different values at certain times.

6. Conclusion

This study concerns the evaluation of the diurnal evolution of radiative forcing caused by atmospheric aerosols on the scale of an urban city located in the heart of the Sahel in West Africa. The results of the simulation carried out using the GAME code showed cooling at the top of the atmosphere and at the surface and then warming of the atmospheric layer in accordance with the literature. The study of diurnal variability sheds light on the influence of solar zenith angle and human activity from sunrise to sunset. The seasonal approach of the study clearly shows the influence of the succession of the dry season characterized by a strong suspension of desert dust from the Sahara desert and the rainy season drained by the humid monsoon flows from guinea golf. This result highlights the

radiative contribution of desert aerosols in the overall radiative balance of Sahelian cities.

Acknowledgements

The authors express their gratitude to International Science Program (ISP) for supporting the BUF 01 research group and allowing to carry out this work.

Conflicts of Interest

The authors declare no conflicts of interest regarding the publication of this paper.

References

- [1] Laurent, B. (2005) Simulation des émissions d'aérosols désertiques l'échelle continentale: Analyse climatologique des émissions du nord-est de l'Asie et du nord de l'Afrique. Ph.D. Thesis, Université Paris, Paris, 12.
- [2] Schütz, L., Jaenicke, R. and Pietrer, H. (1981) Saharan Dust Transport over the North Atlantic Ocean. In: Péwé, T.L., Ed., *Desert Dust: Origin, Characteristics and Effect on Man*, Geological Society of America, Boulder, 87-100.
<https://doi.org/10.1130/SPE186-p87>
- [3] D'Almeida, G.A. (1987) On the Variability of Desert Aerosol Radiative Characteristics. *Journal of Geophysical Research*, **92**, 3017-3026.
<https://doi.org/10.1029/JD092iD03p03017>
- [4] Swap, R., Garstang, M., Greco, S., Talbot, R. and Gac, J.Y. (1992) Sahara Dust in the Amazon Basin. *Tellus Series B*, **44**, 133-149.
<https://doi.org/10.1034/j.1600-0889.1992.t01-1-00005.x>
- [5] Laurent, B., Heinold, B., Tegen, I., Bouet, C. and Cautenet, G. (2008) Surface Wind Accuracy for Modeling Mineral Dust Emissions: Comparing Two Regional Models in Bodélé Case Study. *Geophysical Research Letters*, **35**, L09804.
<https://doi.org/10.1029/2008GL033654>
- [6] Korgo, B., Roger, J.-C. and Bathiebo, J. (2013) Climatology of Air Mass Trajectories and Aerosol Optical Thickness over Ouagadougou. *Global Journal of Pure and Applied Sciences*, **19**, 169-181.
- [7] Roger, J.C., Guinot, B., Cachier, H., Mallet, M., Dubovik, O. and Yu, T. (2009) Aerosol Complexity in Megacities: From Size-Resolved Chemical Composition to Optical Properties of the Beijing Atmospheric Particles. *Geophysical Research Letters*, **36**, L18806. <https://doi.org/10.1029/2009GL039238>
- [8] Favez, O., Cachier, H., Sciare, J., Alfaro, S.C., El-Araby, T.M., Harhash, M.A. and Abdelwahab, M.M. (2008) Seasonality of Major Aerosol Species and Their Transformations in Cairo Megacity. *Atmospheric Environment*, **42**, 1503-1516.
<https://doi.org/10.1016/j.atmosenv.2007.10.081>
- [9] Dubuisson, P., Roger, J., Mallet, M., Dubovik, O., Fischer, H., *et al.* (2004) A Code to Compute the Direct Solar Radiative Forcing: Application to Anthropogenic Aerosols during the Escompte Experiment. *Proceedings of International Radiation Symposium (IRS 2004) on Current Problems in Atmospheric Radiation*, Busan, 23-28 August 2004, 127-130.
- [10] Scott, N.A. (1974) A Direct Method of Computation of the Transmission Function of an Inhomogeneous Gaseous Medium-I: Description of the Method. *Journal of*

- Quantitative Spectroscopy & Radiative Transfer*, **14**, 691-704.
[https://doi.org/10.1016/0022-4073\(74\)90116-2](https://doi.org/10.1016/0022-4073(74)90116-2)
- [11] Roger, J.-C., Mallet, M., Dubuisson, P., Cachier, H., Vermote, E., Dubovik, O. and Despiou, S. (2006) A Synergic Approach for Estimating the Local Direct Aerosol Forcing: Application to an Urban Zone during the Experience sur Site pour Contraindre les Modèles de Pollution et de Transport d'Emission (ESCOMPE) Experiment. *Journal of Geophysical Research*, **111**, D13208.
<https://doi.org/10.1029/2005JD005986>
- [12] Tamnes, K., Tsay, S.-C., Wiscombe, W. and Jayaweera, K. (1988) Numerically Stable Algorithm for Discrete-Ordinate-Method Radiative Transfer in Multiple Scattering and Emitting Layered Media. *Applied Optics*, **27**, 2502-2509.
<https://doi.org/10.1364/AO.27.002502>
- [13] Lacis, A.A. and Oinas, V. (1991) A Description of the Correlated k-Distribution Method. *Journal of Geophysical Research*, **96**, 9027-9064.
<https://doi.org/10.1029/90JD01945>
- [14] Holben, B.N., Eck, T.F., Slutsker, I., Tanré, D., Buis, J.P., Setzer, A., Vermote, E.F., Reagan, J.A., Kaufman, Y.J., Nakajima, T., Lavenue, F., Jankowiak, I. and Smirnov, A. (1998) AERONET—A Federated Instrument Network and Data Archive for Aerosol Characterization. *Remote Sensing of Environment*, **66**, 1-16.
[https://doi.org/10.1016/S0034-4257\(98\)00031-5](https://doi.org/10.1016/S0034-4257(98)00031-5)
- [15] Saha, A., Mallet, M., Roger, J.-C., Dubuisson, P., Piazzola, J. and Despiou, S. (2008) One Year Measurement of Aerosol Optical Properties over an Urban Coastal Site: Effect on Local Direct Radiative Forcing. *Atmospheric Research*, **90**, 195-202.
<https://doi.org/10.1016/j.atmosres.2008.02.003>
- [16] Zhao, C., Liu, X., Leung, L.R. and Hagos, S. (2011) Radiative Impact of Mineral Dust on Monsoon Precipitation Variability over West Africa. *Atmospheric Chemistry and Physics*, **11**, 1879-1893. <https://doi.org/10.5194/acp-11-1879-2011>
- [17] Malavelle, F., Pont, V., Mallet, M., Solmon, F., Johnson, B., Léon, J. and Liousse, C. (2011) Simulation of Aerosol Radiative Effects over West Africa during DABEX and AMMA SOP-0. *Journal of Geophysical Research*, **116**, D08205.
<https://doi.org/10.1029/2010JD014829>
- [18] Mallet, M., Pont, V., Liousse, C., Roger, J.C. and Dubuisson, P. (2006) Simulation of Aerosol Radiative Properties with the ORISAM-RAD Model during a Pollution Event (ESCOMPTE 2001). *Atmospheric Environment*, **40**, 7696-7705.
<https://doi.org/10.1016/j.atmosenv.2006.08.031>
- [19] Zhao, S.M., Hu, B., Du, C.J., Tang, L.Q., Ma, Y.J., Liu, H., Zou, J.N., Liu, Z.R., Wei, J. and Wang, Y.S. (2019) Aerosol Optical Characteristics and Radiative Forcing in Urban Beijing. *Atmospheric Environment*, **212**, 45-53.
<https://doi.org/10.1016/j.atmosenv.2019.05.034>
- [20] Zheng, Y., Che, H.Z., Xia, X.G., Wang, Y.Q., Wang, H., Wu, Y.F., Tao, J., Zhao, H.J., An, L.C., Li, L., Gui, K., Sun, T.Z., Li, X.P., Sheng, Z.Z., Liu, C.H., Yang, X.Y., Liang, Y.X., Zhang, L., Liu, C., Kuang, X., Luo, S., You, Y.C. and Zhang, X.Y. (2019) Five-Year Observation of Aerosol Optical Properties and Its Radiative Effects to Planetary Boundary Layer during Air Pollution Episodes in North China: Inter-comparison of a Plain Site and a Mountainous Site in Beijing. *Science of the Total Environment*, **674**, 140-158. <https://doi.org/10.1016/j.scitotenv.2019.03.418>
- [21] Alam, K., Trautmann, T. and Blaschke, T. (2011) Aerosol Optical Properties and Radiative Forcing over Mega-City Karachi. *Atmospheric Research*, **101**, 773-782.
<https://doi.org/10.1016/j.atmosres.2011.05.007>